**Showcasing research from Professor Hongzhe Sun and Professor Shuofeng Yuan's laboratories, Department of Chemistry and Department of Microbiology, The University of Hong Kong, Hong Kong SAR, P.R. China.**

Orally administered bismuth drug together with *N*-acetyl cysteine as a broad-spectrum anti-coronavirus cocktail therapy

There is an urgent need for safe and effective therapeutic options for COVID-19. This work has demonstrated the oral efficacy of bismuth citrate with *N*-acetyl cysteine (CBS+3NAC) on the suppression of SARS-CoV-2 replication *in vivo*. Importantly, CBS+3NAC inhibits the replication of a panel of epidemic and seasonal coronaviruses through targeting multiple key viral cysteine enzymes in the viral replication cycles. *N*-acetyl cysteine not only stabilises bismuth-containing metallodrugs but also enhances the uptake of bismuth drugs in tissues. The findings provided insights into a new therapeutic approach for viral infections.

As featured in:
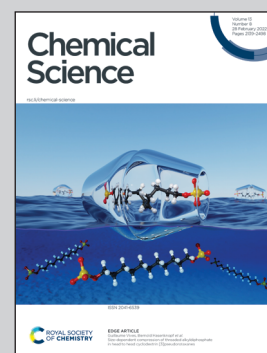
See Shuofeng Yuan, Hongzhe Sun *et al.*, *Chem. Sci.*, 2022, **13**, 2238.

ROYAL SOCIETY
OF **CHEMISTRY**

rsc.li/chemical-science

Check for updates

Orally administered bismuth drug together with *N*-acetyl cysteine as a broad-spectrum anti-coronavirus cocktail therapy†

Runming Wang, ‡[a] Jasper Fuk-Woo Chan,‡[bcdef] Suyu Wang,‡[a] Hongyan Li [a] Jiajia Zhao,[g] Tiffany Ka-Yan Ip,[a] Zhong Zuo, [g] Kwok-Yung Yuen,[bcdef] Shuofeng Yuan *[bcf] and Hongzhe Sun *[a]

The emergence of SARS-CoV-2 variants of concern compromises vaccine efficacy and emphasizes the need for further development of anti-SARS-CoV-2 therapeutics, in particular orally administered take-home therapies. Cocktail therapy has shown great promise in the treatment of viral infection. Herein, we reported the potent preclinical anti-SARS-CoV-2 efficacy of a cocktail therapy consisting of clinically used drugs, *e.g.* colloidal bismuth subcitrate (CBS) or bismuth subsalicylate (BSS), and *N*-acetyl-L-cysteine (NAC). Oral administration of the cocktail reduced viral loads in the lung and ameliorated virus-induced pneumonia in a hamster infection model. The mechanistic studies showed that NAC prevented the hydrolysis of bismuth drugs at gastric pH *via* the formation of the stable component [Bi(NAC)$_3$], and optimized the pharmacokinetics profile of CBS *in vivo*. Combination of bismuth drugs with NAC suppressed the replication of a panel of medically important coronaviruses including Middle East respiratory syndrome-related coronavirus (MERS-CoV), Human coronavirus 229E (HCoV-229E) and SARS-CoV-2 Alpha variant (B.1.1.7) with broad-spectrum inhibitory activities towards key viral cysteine enzymes/proteases including papain-like protease (PL^{pro}), main protease (M^{pro}), helicase (Hel) and angiotensin-converting enzyme 2 (ACE2). Importantly, our study offered a potential at-home treatment for combating SARS-CoV-2 and future coronavirus infections.

Introduction

Severe acute respiratory syndrome coronavirus 2 (SARS-CoV-2) is the causative agent of the Coronavirus Disease 2019 (COVID-19) pandemic which has caused enormous loss of life worldwide.[1,2] Although several vaccines have been approved for

[a]Department of Chemistry, CAS-HKU Joint Laboratory of Metallomics on Health and Environment, The University of Hong Kong, Hong Kong SAR, P. R. China. E-mail: hsun@hku.hk

[b]State Key Laboratory of Emerging Infectious Diseases, Carol Yu Centre for Infection, Department of Microbiology, Li Ka Shing Faculty of Medicine, The University of Hong Kong, Pokfulam, Hong Kong SAR, China. E-mail: yuansf@hku.hk

[c]Department of Clinical Microbiology and Infection Control, The University of Hong Kong-Shenzhen Hospital, Shenzhen, Guangdong Province, China

[d]Hainan Medical University-The University of Hong Kong Joint Laboratory of Tropical Infectious Diseases, The University of Hong Kong, Pokfulam, Hong Kong SAR, China

[e]Academician Workstation of Hainan Province, Hainan Medical University, Haikou, Hainan, China

[f]Centre for Virology, Vaccinology and Therapeutics, Hong Kong Science and Technology Park, Hong Kong SAR, China

[g]School of Pharmacy, Faculty of Medicine, The Chinese University of Hong Kong, Shatin, New Territories, Hong Kong SAR, China

† Electronic supplementary information (ESI) available: Experimental procedures, and supplementary figures. See DOI: 10.1039/d1sc04515f

‡ These authors contribute equally to this work.

emergency use worldwide, it takes a long time to vaccinate the world population. Surprisingly, increasing cases of people getting infected with COVID-19 are reported despite being fully vaccinated. The emergence of SARS-CoV-2 variants associated with enhanced transmissibility and reduced sensitivity to vaccine-induced protection poses a continuous threat to global health.[3] There is an urgent need for safe and effective therapeutic options for COVID-19 which remain scarce.[4] Remdesivir was the first and the only drug approved by the US Food and Drug Administration (FDA) for the treatment of COVID-19.[5] However, patients can only receive remdesivir treatment *via* intravenous route in-hospital[6] as the oral formulation of this drug is still not available. For the majority of COVID-19 patients with mild to moderate disease, an orally available anti-SARS-CoV-2 drug would help to facilitate out-patient treatment and reduce the burdens of healthcare facilities. Indeed, the US government recently announced to invest US$3.2 billion for the development of antiviral drugs to treat coronavirus infection, especially oral drugs that can be taken at home earlier in the course of the disease (https://www.wsj.com/articles/u-s-to-invest-more-than-3-billion-in-covid-19-antiviral-development-11623945647).

The combination of two or more drugs (*i.e.*, cocktail therapy) has been commonly recommended in clinic for the treatment of

virus infection.[4,7,8] In this work, we demonstrated that combinatorial bismuth drugs colloidal bismuth subcitrate (CBS) or bismuth subsalicylate (BSS) and *N*-acetyl-L-cysteine (NAC) potently decreased viral lung loads and the virus-associated pathology following oral administration in Syrian hamster infection model and exhibit broad-spectrum anti-CoV activities. Further mechanistic studies unveiled that NAC could not only stabilize CBS at stomach-like conditions but also enhance uptake of bismuth drugs in tissues (*e.g.* lung) through oral administration. Bismuth subsequently suppressed virus replication by inhibiting multiple essential viral enzymes. The combination therapy comprising a metallodrug CBS (or BSS) and a thiol-containing drug NAC served as a promising orally administrated broad-spectrum anti-CoV regimen and possibly therapeutic use for the treatment of COVID-19 patient.

Results

Combinatorial a bismuth drug and NAC exhibit broad-spectrum anti-CoVs potency both *in vitro* and *in vivo*

We previously verified the *in vivo* anti-SARS-CoV-2 potency of bismuth drug ranitidine bismuth citrate (RBC) *via* the intraperitoneal injection.[9] To reduce the high-risk exposure use of drugs, we first evaluated the efficacy of RBC after intraperitoneal administration in a well-established golden Syrian hamster model of SARS-CoV-2 infection.[10] CBS instead of RBC was used in this study to rule out the indefinite effects of low levels of probable human carcinogens present in ranitidine byproduct.[11] To achieve optimal antiviral performance, multiple doses of bismuth drugs were given in the dosing regimen. A group of animals ($n = 8$ per group) were administered with CBS by oral gavage on day −2, −1, and 6 hours before the intranasal challenge of SARS-CoV-2 on day 0, and day 1 post-infection (Fig. 1A). A control group was treated with vehicle only using the same route and timing as the CBS-treated group. The viral loads in the lungs in the respective group were then determined at 2 day post-infection (dpi) when the viral loads escalated with prominent histopathological changes. Surprisingly, neither statistically significant reduction in either lung viral load or expression of proinflammatory gene IL-6, was observed between the vehicle and CBS group (Fig. 1B and C), indicative of the poor systemic absorption of bismuth drugs *via* oral administration. Given that Bi^{3+} is highly thiophilic[12] and some biological thiols were shown to facilitate bismuth uptake and delivery through thiol-exchange,[13,14] we hypothesized that thiol-containing small molecules may boost the oral antiviral efficacy of bismuth drugs through improvement of the systemic absorption of bismuth. Combinatorial bismuth drugs with NAC, an FDA-approved drug that is commonly used as a mucolytic in patients with pneumonia, as well as various other medical conditions such as paracetamol overdose,[15] may therefore exhibit potent anti-SARS-CoV-2 efficacy.

To avoid the potential impact of excessive NAC on antiviral evaluation,[16] CBS was co-administered with 3 mol eq. NAC (denoted as CBS + 3NAC hereafter) for the following animal-based and cell-based studies. Under identical conditions, combinatorial CBS + 3NAC led to a 15.9(±4.6)-fold reduction in

mean copy numbers of lung SARS-CoV-2 RNA compared with vehicle group, with statistically significant difference ($P < 0.0001$, Kruskal–Wallis with Dunn's multiple comparison test) between them while no statistically significant difference was observed among vehicle, CBS and NAC group (Fig. 1B). In parallel, the antiviral potency of BSS was substantially improved by 6.1(±3.3) folds after co-administration of 3 mol eq. NAC ($P < 0.005$, Kruskal–Wallis with Dunn's multiple comparison test, Fig. 1D). Intriguingly, CBS + 3NAC treatment led to a significantly decreased IL-6 level by 14.4 folds compared with that from the vehicle group, whereas CBS-treatment also caused lowered but statistically non-significant change in IL-6 level (Fig. 1C). Immunoreactivity against SARS-CoV-2 antigen was used to further compare the lung samples between the three different treatment groups. Using immunofluorescence staining (Fig. 1E and F), the superior antiviral effect of CBS + 3NAC was further depicted by prominently lowered SARS-CoV-2-NP antigen signal (12.33(±8.51) NP^+ cells per view) in alveolar tissue of hamster lungs of CBS + 3NAC-treated group in comparison to that in the non-treated group (92.33(±12.50) NP^+ cells per view), CBS-treated (68.00(±6.08) NP^+ cells per view) or NAC-treated group (85.67(±11.59) NP^+ cells per view). Above results provided robust evidence of potential of combinatorial bismuth drugs CBS and thiol-containing drugs NAC following the oral administration to contain SARS-CoV-2 in the highly susceptible Syrian hamster model.

At the end of the experimental period, signs of lethargy, ruffled fur, hunched back posture and rapid breathing occurred in infected hamsters in vehicle group, whereas these adverse clinical signs and symptoms were significantly ameliorated in CBS + 3NAC-treated group and mildly mitigated in CBS-treated group. The severity of lung damage was further examined by performing histological examination of hematoxylin and eosin (H&E) staining in hamster lung tissues. Consistent with the observation of clinical signs, infected hamsters receiving vehicle developed large areas of consolidation, cell infiltrations in endothelium of blood vessels as well as peribronchiolar regions (Fig. 1G). In contrast to vehicle group, these severe pathological changes were greatly prevented in CBS + 3NAC-treated hamsters as revealed by the estimated lung histology scores diminished from 8.67(±0.67) to 2.67(±0.67) (Fig. 1H), suggesting oral treatment of CBS + 3NAC mitigated the risk of progression to severe disease and accelerated recovery. In addition, we administered CBS + 3NAC at converted dosage based on body surface area to uninfected Balb/c mice under identical therapeutic condition, and found only slightly elevated but a reversible change in the level of blood urea nitrogen (BUN) and creatinine while no other pathogenic signs were observed on this regimen (Fig. S1†).

Importantly, we validated that CBS + 3NAC showed broad-spectrum potency against SARS-CoV-2 and other human-pathogenic CoVs. CBS + 3NAC treatment reduced SARS-CoV-2 yield up to >3 × $\log_{10}$ in the Vero E6 cell culture supernatant (Fig. 1I and Table S1†) while NAC alone exhibited negligible anti-SARS-CoV-2 activity at even up to 2000 μM under identical conditions (Fig. S2†). The EC_{50} of CBS + 3NAC was estimated to be 5.83(±0.57) μM according to plaque reduction assay, which
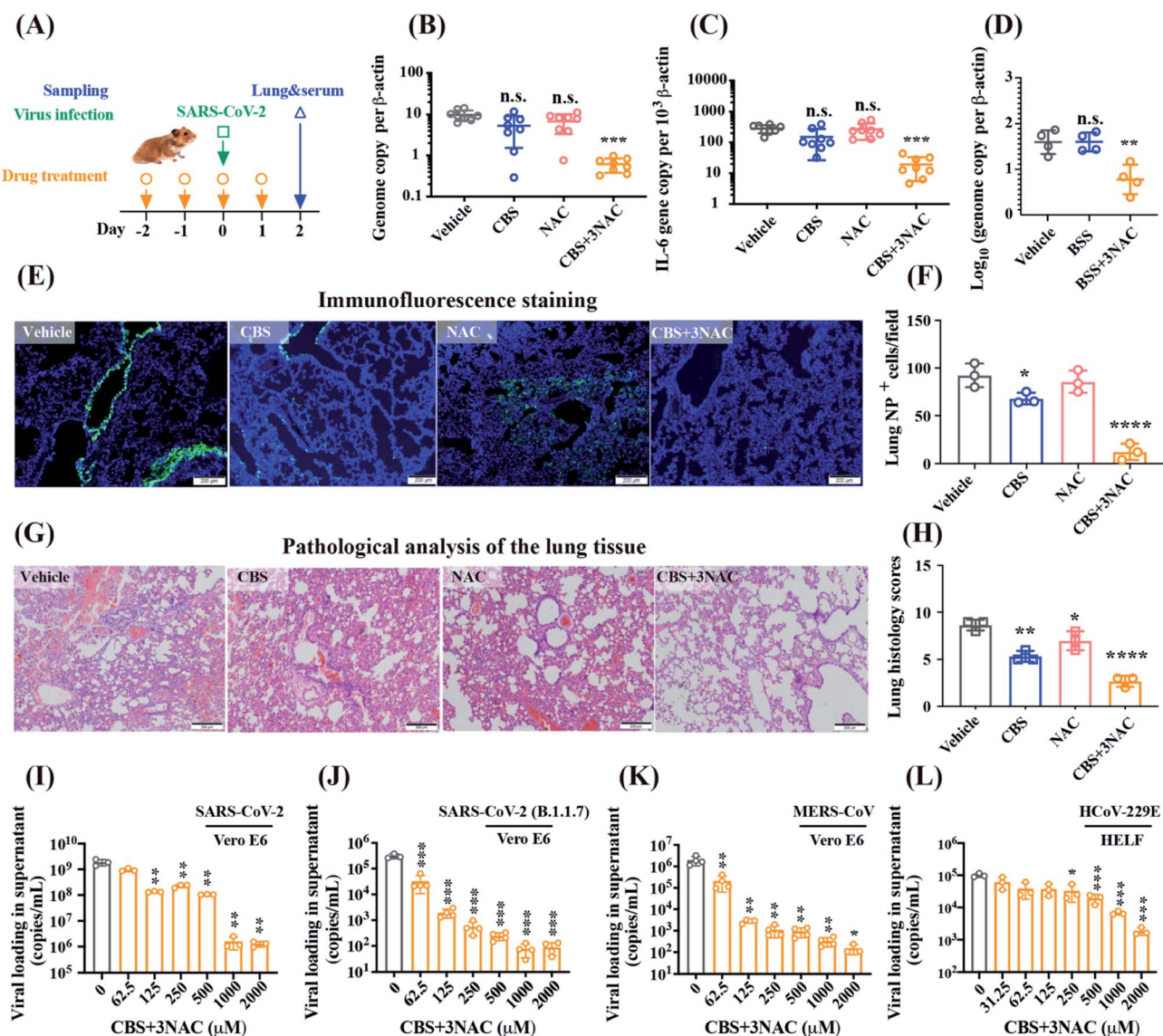
Fig. 1 Combinatorial CBS and NAC exhibit broad-spectrum anti-CoVs potency both *in vitro* and *in vivo*. (A) Scheme depicting the therapeutic treatment *via* oral administration of vehicle, CBS (300 mg kg^{-1}), BSS (300 mg kg^{-1}), NAC (370 mg kg^{-1}), CBS (300 mg kg^{-1}) + 3NAC (370 mg kg^{-1}) or BSS (300 mg kg^{-1}) + 3NAC (405 mg kg^{-1}), given on day −2, −1, 0 and 1. The hamsters were challenged by virus on day 0. Tissue samples were collected on day 2. (B) Viral yield in lung tissues of hamsters ($n = 8$) receiving treatment of vehicle, CBS, NAC, and CBS + 3NAC, respectively. (C) Cytokine IL-6 gene expression level in lung tissues of hamsters ($n = 8$) receiving treatment of vehicle, CBS, NAC, and CBS + 3NAC, respectively. (D) Viral yield in lung tissues of hamsters ($n = 4$) receiving treatment of vehicle, BSS, and BSS + 3NAC, respectively. (B−D) Data were shown as mean ± SD. Statistical significance was shown between the vehicle group and drug-treatment group, which was calculated using Kruskal−Wallis with Dunn's multiple comparison test. ***$P < 0.001$, ***$P < 0.005$, n.s., no significant difference. (E) Representative images of the viral N protein distribution in lung tissue sections from groups of vehicle control, CBS, NAC, and CBS + 3NAC, respectively, at 2 d.p.i. (F) Quantification of NP-positive cells from randomly selected 800 × 800-pixel fields ($n = 4$) in lung tissues (one-way analysis of variance, ANOVA). ****$P < 0.0001$, *$P < 0.05$. Data were shown as mean ± SD. (G) Representative images of H&E-stained lung tissue sections from vehicle control, CBS, NAC, and CBS + 3NAC, respectively. (H) Semiquantitative histology scores given to each lung tissue by grading the severity of damage in bronchioles, alveoli and blood vessels and accumulating the total scores. The histological score of mock infection was set as '0'. Data were shown as mean ± SD. Statistical significance was shown between the vehicle group and drug-treatment group, which was calculated using an unpaired two-tailed Student's *t*-test, ****$P < 0.0001$, **$P < 0.01$, *$P < 0.05$. (I−L) CBS + 3NAC suppressed replication of human-pathogenic coronaviruses in human cellular models in a dose-dependent manner ($n = 3$), specifically for (I) SARS-CoV-2 in Vero E6 cells (J) SARS-CoV-2 (B.1.1.7 variant) in Vero E6 cells (K) MERS-CoV in Vero E6 cells and (L) HCoV-229E in HELF cells. Viral load in the cell culture supernatant was quantified by qPCR with reverse transcription (RT-qPCR). Data were shown as mean ± SD. All statistical analyses were compared with the control group (0 μM) and statistical significance was shown between the vehicle group and drug-treatment group, which was calculated using an unpaired two-tailed Student's *t*-test, ***$P < 0.001$, **$P < 0.01$, *$P < 0.05$.

was comparable to that of CBS ($EC_{50} = 4.6(\pm 0.4)$ μM),[9] showing the combined use of CBS with NAC did not compromise the antiviral potency of bismuth drugs. Immunofluorescence staining assay further concreted the anti-SARS-CoV-2 potency of CBS + 3NAC as evidenced by prominently lowered viral NP antigen in CBS + 3NAC-treated group (11.75%) in comparison to that in the non-treated group (64.5%), CBS-treated (37.25%) or NAC-treated group (59.75%) (Fig. S3†). Significantly, CBS + 3NAC treatment remarkably reduced viral yield by about 2 × $\log_{10}$ and about 4 × $\log_{10}$ against SARS-CoV-2 Alpha variant (B.1.1.7)[3,17] and MERS-CoV-infected Vero E6 cell culture supernatants, respectively, and up to >1.5 × $\log_{10}$ in the cell culture supernatants of hCoV-229E-infected human embryonic lung fibroblasts (HELF) (Fig. 1J, K and Table S1†). The results indicated that CBS + 3NAC potentially provided a broad-spectrum antiviral option against epidemic and seasonal coronaviruses.

N-Acetyl cysteine stabilizes bismuth drugs in vitro and promotes absorption of bismuth drugs in vivo

To ascertain how thiol-containing drugs improved the oral availability of bismuth drugs, we first validated whether NAC stabilized bismuth drugs in simulated gastric fluid (pH 1.2), Dulbecco's phosphate buffer saline (PBS, pH 7.4) and sodium bicarbonate buffer (pH 9.2). The combinatorial use of CBS with n molar equivalents of (n mol eq.) NAC was denoted as CBS + nNAC hereafter. CBS was a clear solution at biological pH, but when CBS was added into simulated gastric juice buffer (pH 1.2), a white precipitate was formed instantly, with less than 10% bismuth found in the supernatant upon standing for 1 hour (Fig. 2A and S4†). In contrast, NAC prevented the precipitation of CBS in a dose-dependent fashion, with approximately 100% bismuth remained in the supernatant in the presence of either 3 or 10 mol eq. NAC. In addition, NAC could similarly prevent hydrolysis of CBS even at pH 9.2. Furthermore, NAC could also prevent the hydrolysis of other bismuth drugs, including RBC, BSS, and bismuth subgallate (BSG), under acidic conditions (Fig. S4†). This was possibly owing to the formation of a stable bismuth thiolate complex, $[Bi(NAC)_3]$ as previously reported.[18] The formation of $[Bi(NAC)_3]$ components was further confirmed by UV-titration and ESI-MS (Fig. S5 and S6†). We subsequently estimated bismuth permeability through the simulated gastrointestinal barrier in the presence of egg lecithin in dodecane (1% w/v) using a modified parallel artificial membrane permeability assay (PAMPA). After reaching equilibrium state in PBS (iso-pH 1.2), the cumulative permeated bismuth was increased from 16.95, 15.24 and 18.80 ng cm^{-2} to 24.91, 19.77 and 24.13 ng cm^{-2} for CBS, RBC and BSS, respectively, in the presence of 10 mol eq. NAC (Fig. 2B). This suggests the chemical stability and permeability of CBS as well as related bismuth drugs could be potentially modulated through a combined use of a thiol-containing drug NAC.

We further characterized the bismuth uptake via gastrointestinal segments in the absence or presence of NAC by the human intestinal epithelial cancer cell line (Caco-2)[19] and a modified ex vivo everted gut sac model (at physiological pH 7.4).[20] From Caco-2 permeability assay (Fig. 2C), bismuth intestinal permeation was moderately elevated within 60 min in the presence of 10 mol eq. NAC and the cellular accumulation of bismuth was increased from 0.33($\pm$0.02)% to 0.40($\pm$0.02)% (Fig. 2D). The human intestinal epithelial cell permeability (P_{app}) of CBS was increased significantly from 1.73($\pm$0.02) × 10^{-7} to 2.24($\pm$0.21) × 10^{-7} cm s^{-1} in the presence of 10 mol eq. NAC (Fig. 2E). The improved intestinal absorption of bismuth by NAC was further demonstrated in the everted sac model that the cumulative bismuth permeated was remarkably boosted from 14.68($\pm$4.12) to 30.21($\pm$5.50), 64.98($\pm$12.56) and 98.61($\pm$3.06) ng cm^{-2} within 60 min when CBS was used in combination with 1, 3 and 10 mol eq. NAC, respectively (Fig. 2F). Collectively, we demonstrate that the oral absorption of bismuth drugs could be potentially improved by co-administering with NAC.

The pharmacokinetic properties of CBS were subsequently evaluated in the absence and presence of NAC. We administrated CBS without or with different amounts of NAC to Balb/c mice, and found that the blood bismuth concentration was prominently increased from 225.75($\pm$86.05) to 372.04($\pm$162.12) and 447.29($\pm$57.02) μg L^{-1} after 0.5 hour exposure, and from 87.27($\pm$21.46) to 332.76($\pm$89.61) and 1459.58($\pm$167.46) μg L^{-1} after 1 hour exposure when 150 mg kg^{-1} CBS was orally co-administered with 3 mol eq. (180 mg kg^{-1}) and 10 mol eq. (610 mg kg^{-1}) NAC, respectively (Fig. 2G). We next profiled the mean blood bismuth concentration versus time curves after a single oral dose of either CBS (150 mg kg^{-1}) and its combination with 10 mol eq. NAC (610 mg kg^{-1}) in rats. As shown in Fig. 2H, both CBS and CBS + 10NAC groups displayed a double-peak profile, which is similar to that reported previously.[21] For CBS group, the blood bismuth level decreased from the first peak value of 277.69 μg L^{-1} at around 0.5 h, as seen in a previous human study,[22] and reached to C_{max} of 447.06($\pm$132.39) μg L^{-1} at 4 h, with a value of area under the curve over 0 to 12 h ($AUC_{0 \to 12 h}$) of 1316($\pm$474.00) h μg L^{-1}. Remarkably, NAC served to increase the peak blood concentration of bismuth to 758.81($\pm$251.74) μg L^{-1} and appeared with a prolonged T_{max} (Table S2†), resulting in a significant elevation in $AUC_{0 \to 12 h}$ of 2750($\pm$1151.99) h μg L^{-1}. Additionally, NAC significantly improved bismuth accumulation in the lung (CBS: 552.15($\pm$104.97) ng per tissue verses CBS + 10NAC: 1056.62($\pm$196.31) ng per tissue) and kidney (CBS: 6839.76($\pm$1652.30) ng per tissue vs. CBS + 10NAC: 18 788.60($\pm$6768.42) ng per tissue), and moderately facilitated the bismuth uptake in other organs i.e., spleen and liver, as revealed by the biodistribution profile of bismuth in different organs at 24 hour (Fig. 2I). Taken together, both the in vitro and in vivo pharmacokinetics data consistently demonstrated that the co-administration of CBS with NAC led to a remarkably improved bismuth uptake profile in both blood and different organs, which significantly improved the oral availability of bismuth drug for combating SARS-CoV-2 infection.

Bismuth drugs exhibit antiviral potency through targeting multiple conserved key cysteine proteases/enzymes in SARS-CoV-2

The mode of action of CBS + 3NAC against SARS-CoV-2 was examined by a time-of-drug-addition assay in a single viral
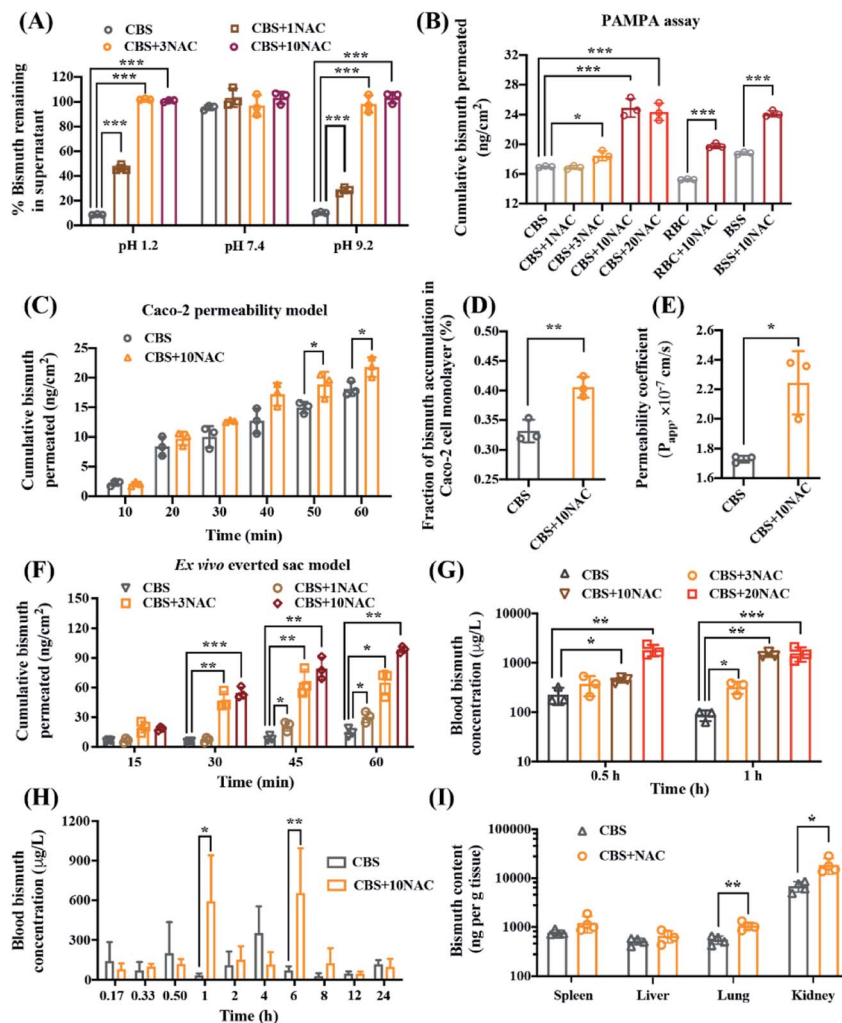
Fig. 2 *N*-Acetyl cysteine stabilizes CBS *in vitro* and promotes absorption of bismuth drug *in vivo*. (A) *In vitro* chemical stability of CBS (2.5 mM) at pH 1.2 (left), pH 7.4 (middle) and pH 9.2 (right) in the presence of escalating amounts of NAC. The percentage of remaining bismuth was calculated from the ratio of bismuth content in supernatant measured at 1 h to 0 h ($n = 3$). (B) Cumulative amount of bismuth in acceptor compartments at acidic iso-pH 1.2 for three bismuth drugs in the absence and presence of appropriate amounts of NAC using a PAMPA permeability assay ($n = 3$). (C) Cumulative amount of bismuth in acceptor compartments over time for CBS (150 μM) in the absence and presence of 10NAC (1.5 mM) in a Caco-2 cell monolayer model ($n = 3$). (D) Bismuth accumulation in Caco-2 cell monolayer ($n = 3$). (E) The apparent permeability coefficient (P_{app}, cm s^{-1}) of CBS (150 μM) and CBS (150 μM) + 10NAC (1.5 mM) through the Caco-2 monolayer ($n = 3$). (F) Cumulative amount of bismuth transported through duodenum verse time for CBS (200 μM) in the presence of escalating amounts of NAC in the everted rat intestinal sac model ($n = 3$). (G) Blood bismuth concentrations at 1 hour and 2 hour after oral administration to Balb/c mice of CBS (150 mg kg^{-1}) in the presence of escalating amounts of NAC ($n = 3$). (H) Mean blood bismuth concentration *versus* time profile of CBS and CBS (150 mg kg^{-1}) + 10NAC (610 mg kg^{-1}) after oral administration in SD rats ($n = 5$ for each time interval). (I) Distribution of bismuth in different organs after oral administration of CBS and CBS + 10NAC in SD rats ($n = 5$). The samples were collected at 24 hours after drug administration from the same batch of rats in (H). (A–I) Measurement of drug concentration were based on metal content by using inductively coupled plasma mass spectroscopy (ICP-MS). Data are shown as mean ± SD. Statistical significance was calculated using an unpaired two-tailed Student's *t*-test, ***P < 0.001, **P < 0.01, *P < 0.05.

replication cycle. Treatment with CBS + 3NAC robustly hindered the SARS-CoV-2 infection as manifested by $3.54 \times \log_{10}$ and $1.73 \times \log_{10}$ decline in viral load when CBS + 3NAC was added during co-incubation and post-entry stages, respectively; while it was observed that CBS + 3NAC barely interfered with viral attachment (*i.e.* pre-incubation, Fig. 3A). Considering the marginal influence of NAC alone on viral replication, it was suggested that CBS + 3NAC interferes with multiple steps including SARS-CoV-2 internalization and/or post-entry events. We first

observed that CBS + 3NAC interfered the SARS-CoV-2 entry *via* inhibiting the activity of angiotensin-converting enzyme 2 (ACE2), a key receptor for the SARS-CoV-2 that causes COVID-19. Specifically, as shown in Fig. S7 and Table S3,† CBS + 3NAC showed inhibitory effects on ACE2 activity at a comparable level of NAC itself; while CBS barely displayed anti-ACE2 potency, which suggested the chelating effect of NAC primarily contributed to the inhibition of ACE2 activity by CBS + 3NAC. To explore the impact of CBS + NAC on post-entry steps of viral
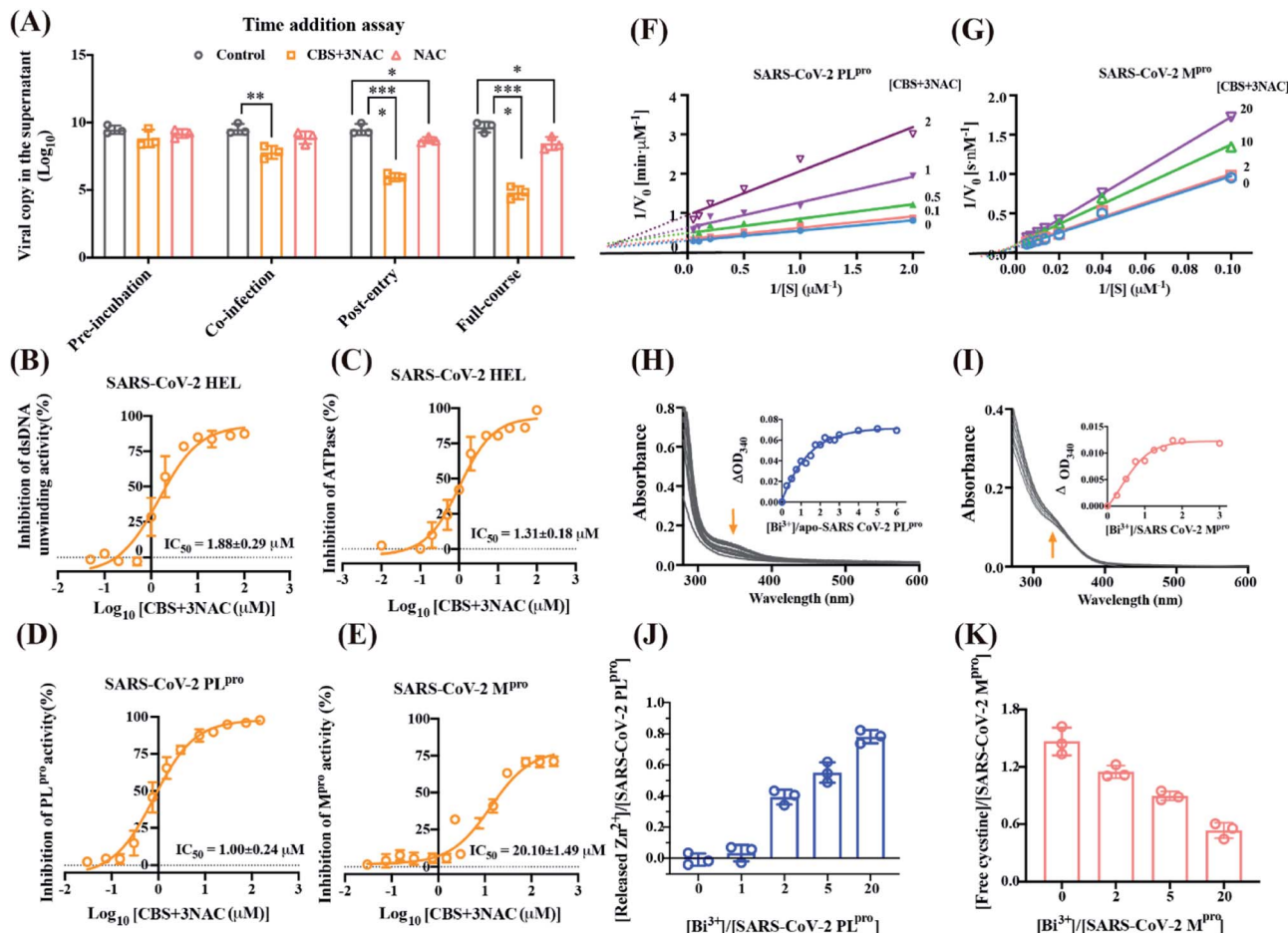
Fig. 3 Bismuth drug exhibits antiviral potency through targeting multiple conserved key cysteine proteases/enzymes in SARS-CoV-2. (A) Virus yields in the supernatant of all groups in a time-of-drug-addition assay, quantified by qRT-PCR at 9 h.p.i. ($n = 3$). Data are shown as mean ± SD. One-way ANOVA was used to compare the treatment groups with the vehicle control group (0 μM). ****$P < 0.0001$, **$P < 0.01$, *$P < 0.05$. (B–E) Inhibition of CBS + 3NAC on (B) dsDNA unwinding activity of SARS-CoV-2 Hel, (C) ATPase activity of the SARS-CoV-2 Hel, (D) SARS-CoV-2 PL^{pro} activity, (E) SARS-CoV-2 M^{pro} activity ($n = 3$). (F and G) Lineweaver–Burk plots showing the kinetics of CBS + 3NAC inhibition on (F) SARS-CoV-2 PL^{pro} activity (G) SARS-CoV-2 M^{pro} activity. The effect of CBS + 3NAC on the enzymes was determined from the double reciprocal plot of 1/rate (1/V) versus 1/substrate concentration in the presence of varying concentrations of CBS + 3NAC. The Ki values were calculated by the inter-section of the curves obtained by plotting 1/V versus inhibitor concentration for each substrate concentration. (H–I) Difference UV-vis spectra for titration of various molar equivalents of Bi^{3+} with (H) apo-SARS-CoV-2 PL^{pro} and (I) SARS-CoV-2 M^{pro}. The insets show a titration curve plotted at ∼340 nm against the molar ratio of (H). [Bi^{3+}]/[apo-SARS-CoV-2 PL^{pro}] and (I) [Bi^{3+}]/[SARS-CoV-2 M^{pro}]. The assays were performed twice and representative data are shown. (J) Released Zn^{2+} from SARS-CoV-2 PL^{pro} after incubation with Bi^{3+} at escalating concentrations ($n = 3$). (K) Semi-quantification of free cysteine in SARS-CoV-2 M^{pro} after incubation with Bi^{3+} on an Ellman's assay ($n = 3$). (A–E, J and K) Data are shown as mean ± SD.

replication, we verified the comparable inhibitory effects of CBS + 3NAC to CBS on SARS-CoV-2 Hel duplex unwinding activity with IC$_{50}$ of 1.24(±0.02) μM for CBS, 1.88(±0.29) μM for CBS + 3NAC and ATPase activity with IC$_{50}$ of 1.88(±0.12) μM for CBS, and 1.31(±0.18) μM for CBS + 3NAC (Fig. 3B and C). We next investigated the potential inhibition of CBS + 3NAC on the two distinctive conserved cysteine proteases encoded by the SARS-CoV-2 genome, papain-like protease (PL^{pro}, a domain within Nsp3) possessing a conserved structural Zn^{2+} in the finger subdomain and chymotrypsin-like main protease (M^{pro}, Nsp5), both of which are requisitely responsible for the proteolytic cleavage of the two large replicase polyproteins (ORF1ab and ORF1a) for the viral genome replication,[23] and some biological

events beyond. By using fluorescence resonance energy transfer (FRET)-based cleavage assays, the activity of SARS-CoV-2 PL^{pro} and SARS-CoV-2 M^{pro} were assessed with a peptide substrate of RLRGG-AMC and Dabcyl-KTSAVLQSGFRKM-E(Edans)-NH$_2$, respectively. As shown in Fig. 3D, E and S8, ESI,† CBS + 3NAC and CBS inhibited SARS-CoV-2 PL^{pro} with IC$_{50}$ of 1.00(±0.24) μM and 1.02(±0.25) μM respectively, and SARS-CoV-2 M^{pro} with IC$_{50}$ of 21.10(±1.49) μM and 22.25(±2.23) μM, respectively, in a dose-dependent fashion while NAC exhibited negligible inhibitory activity at comparable concentrations (Table S3†). This suggested the inhibitory effects of CBS + 3NAC stemmed principally from Bi^{3+} ions. Increasing concentrations of CBS + 3NAC revealed an unchanged value of maximum velocity (V_{max})

value at 12.48 ± 0.53 nM s^{-1}, whereas an increase in apparent Michaelis–Menten constant (K_m) from 176.4 to 320.0 nM was observed, indicative of a typical competitive inhibition of CBS + 3NAC on SARS-CoV-2 M^{pro} activity with an inhibition constant (K_i) of 6.20 ± 0.40 μM; while CBS + 3NAC showed a mixed inhibition on SARS-CoV-2 PL^{pro}, possibly owing to the binding of Bi^{3+} to its zinc finger domain as well as to its active site cysteine (Fig. 3F and G).

We monitored the binding of Bi^{3+} to the cysteine residues of SARS-CoV-2 PL^{pro} and SARS-CoV-2 M^{pro} as evidenced by appearance of characteristic Bi–S ligand-to-metal charge transfer (LMCT) band at ~340 nm when 20 mol eq. Bi^{3+} (as CBS) was titrated to respective proteins (Fig. S9†) with $t_{1/2}$(PL^{pro}) of 62.07 min, and $t_{1/2}$(M^{pro}) of 3.38 min. Upon the escalation of Bi^{3+}, the absorption at 340 nm increased and then leveled off at a molar ratio of [Bi^{3+}]/[SARS-CoV-2 PL^{pro}] of ~3 and [Bi^{3+}]/[SARS-CoV-2 M^{pro}] of ~1, with estimated dissociation constant (K_d) of 1.13 μM and 0.60 μM, respectively (Fig. 3H and I). The binding of Bi^{3+} led to the release of ~0.78 eq. Zn^{2+} from SARS-CoV-2 PL^{pro}, which in part contributed to the inhibition of its activity (Fig. 3J). Additionally, the amount of free cysteine in SARS-CoV-2 M^{pro} was found to decrease by ~1 mol eq. upon the binding of Bi^{3+} as determined by Ellman's assay. Coincided with previous data (Fig. 3K), these results imply that bismuth drugs, i.e., CBS + 3NAC, block multiple biological events during the virus entry and post-entry stage, through binding and functional inactivation of crucial viral receptor, i.e. ACE2 or cysteine proteases, i.e., PL^{pro}, M^{pro} and Hel, eventually leading to the prohibition of coronavirus replication.

Discussion and conclusion

Bismuth drugs, including CBS and RBC, have been clinically used together with antibiotics as a quadruple therapy to eradicate *Helicobacter pylori*, which causes peptic ulcers and other diseases of the gastrointestinal tract.[24–26] RBC was found to be highly potent against SARS-CoV-2 *in vitro* and in a hamster model for COVID-19 through intraperitoneal administration.[9] However, the anti-SARS-CoV-2 efficacies of bismuth drugs through oral administration have not been evaluated. In current study, we assessed the antiviral potency of combinatorial bismuth drugs, i.e., CBS and BSS, with a thiol-containing drug NAC against SARS-CoV-2 in cell infection models and in a Syrian hamster model of SARS-CoV-2 infection *via* the oral administration route. Our data bolstered the notable oral efficacy of CBS + 3NAC as well as BSS + 3NAC on the suppression of SARS-CoV-2 replication *in vivo*, as supported by the substantial reduction of viral loading in the lungs based on viral RNA genome copy number (Fig. 1A–F). The combinatory CBS and NAC also served to ameliorate the virus-associated lung pathology after oral administration (Fig. 1G and H). Notably, we also showed in this study that CBS + 3NAC exhibited a broad-spectrum anti-CoVs activity by suppressing the replication of a SARS-CoV-2 variant, SARS-CoV-2 (B.1.1.7) and a range of epidemic and seasonal CoVs including MERS-CoV, and hCoV-229E in human cellular models (Fig. 1H–K). Importantly, in comparison to other heavy metals, bismuth is a 'green' metal[27] and Bi^{3+} is

selectively toxic to certain human pathogens rather than human hosts.[13] Specifically, bismuth drugs have been used in clinic for decades with well-documented safety profiles.[28,29] Nephrotoxicity has been considered as the major adverse effect of high-dose intake of CBS.[30,31] We provided data to substantiate that little or reversible renal damage following the intake of CBS (500 mg kg^{-1}) + 3NAC (580 mg kg^{-1}) for 4 consecutive days in mice as adjudged by the BUN and creatinine levels in a 28 day duration. Considering the emergence of SARS-COV-2 variants[32] and resistance to anti-SARS-CoV-2 agents, e.g., remdesivir,[33] bismuth drugs and related metallodrugs would have great potentials to serve as a broad-spectrum antiviral agents for the treatment of COVID-19 patients.

The main exposure route for currently clinically used bismuth drugs is *via* oral administration. However, bismuth compounds are considered to have poor to moderate systemic absorption following ingestion. The low bioavailability of bismuth was also documented by the measured absorption of bismuth from CBS, BSS and bismuth subnitrate (BSN) in the rat small intestine, which was lower than 1%.[34–37] This was largely owing to the low solubility including hydrolysis of bismuth drugs in gastric acid environment. CBS possesses a stable di-nuclear unit, [Bi(citrate)$_2$Bi]$^{2-}$ with additional O^{2-}, OH$^-$ and H$_2$O ligands. The subunits further assemble *via* bridging citrate ligands and a network of hydrogen bonds involving citrate, ammonium ions and water.[38] The solubility of CBS in water is dramatically affected by pH, from >70 mg mL^{-1} at pH 7 to only about 1 mg mL^{-1} at pH 3.[39] In particular, CBS undergoes hydrolysis upon acidification when chloride ion was present in dilute solutions (e.g. in gastric juice environment), to form white precipitates of BiOCl and bismuth citrate,[40] which could be remarkably prohibited in the presence of thiol-containing bioligands, owing to the formation of highly stable and soluble bismuth-thiol complexes in aqueous medium.[14] For example, Williams et al.[37] reported previously that cysteine and glutathione (GSH) prevented the precipitation of bismuth drugs at pH 2.

In the present study, precipitation was observed when CBS was added into simulated gastric juice buffer (pH 1.2) (Fig. 2A and S4†). In contrast, the precipitation was almost completely prevented when CBS was mixed with NAC (Fig. 2A and S4†) and importantly, the uptake profile of Bi^{3+} was substantially promoted both *in vitro* and *in vivo* in a dose-dependent manner (Fig. 2B–I). This was due to the formation of a highly stable and water-soluble Bi^{3+} thiolate complex, [Bi(NAC)$_3$], which was the likely active component of CBS + 3NAC. In principle, It is thermodynamically favourable to bind thiolate ligands to Bi^{3+} to form bismuth thiolate complexes.[41] When Bi^{3+} was mixed with 3 or more mol eq. NAC, [Bi(NAC)$_3$] would form rapidly,[14,18,42] which was further confirmed by UV spectroscopy (Fig. S5 and S6†). A previous study using EXAFS demonstrated that Bi^{3+} only coordinates to thiolate sulphur in [Bi(NAC)$_3$] both in solution and solid with an average Bi–S bond length of 2.55 Å.[18] The thiolated bismuth such as [Bi(NAC)$_3$] could undergo fast thiol exchange in glycoproteins,[43,44] which potentially increase both the lipophilicity and membrane permeability of bismuth as others indicated,[45,46] thus further enhancing the oral absorption of bismuth drugs.

Bi^{3+} is a borderline metal ion and thus, the thiophilic nature of Bi^{3+} is a clear manifestation that thiolate-containing biological molecules (*e.g.* cysteine residues) are likely to be their potential targets. We have showed previously that bismuth drugs could feasibly target Zn^{2+}-cysteine site(s) of proteins in pathogens such as the zinc finger domain (CXXC type) of SARS-CoV-2/SARS-CoV helicase (Hel, Nsp13),[9,47] catalytic zinc site of NDM-1 (ref. 48) and zinc-binding chaperonin GroES[49,50] as well as cysteine protease such as caspases 3 and caspase 9,[51] and inactive the enzymes. This subsequently leads to the disruption of the downstream biological functions of those proteins. It was deduced that Bi^{3+} has potential pleiotropic effects to target multiple biological pathways through binding to key proteins, in particular key cysteine site(s) of viral proteins. We showed in this study that the inhibitory effect of CBS + 3NAC was largely manifested in post-entry stage of viral replication (Fig. 3A). The pan-inhibitory activity of bismuth drugs against various CoVs possibly stemmed from their selective abilities to target multiple viral enzymes in the viral replication cycles. Our combined data demonstrated that CBS as well as related metallodrugs could significantly inactivate the viral cysteine proteases through either binding to the key cysteine residue in the active sites (PL^{pro} and M^{pro}) or replace the key zinc ions in the structural zinc-finger domains (PL^{pro} and Hel) (Fig. 3B–K and Table S3†). Intriguingly, we herein also found that CBS + 3NAC showed inhibitory activity towards an essential human protein ACE2 (Fig. S7A and Table S3†) which was tightly associated with viral entry of SARS-COV-2.[52] ACE2 is a zinc protein that is devoid of cysteine residues in its active site. Bi^{3+} itself showed diminished binding affinity well as inhibitory potency to those type of proteins, as evidenced by previous report[53] and current study (Fig. S7B and Table S3†). It was highly possible that the NAC from the formed kinetically labile $[Bi(NAC)_3]$, chelated to zinc ions at the active site of ACE2, thus inhibiting its activity. In this sense, the combinatory CBS + 3NAC possibly exhibited wider spectrum of inhibitory activity towards viral proteins in CoVs than bismuth drugs alone. A proposed molecular mechanism of action of CBS + 3NAC scheme was shown in Scheme 1.

NAC is available as an intravenous (IV), oral, and inhalable drug.[54,55] It is generally safe with few side effects clinically, and also exhibits anti-oxidant, anti-inflammatory, and immunomodulating effects.[56,57] Although the anti-SARS-CoV-2 activity contributed predominantly from Bi^{3+} as manifested by current and previous study,[9] NAC still played an essential role in current combinatory therapy. First, NAC stabilized Bi^{3+} in gastric environment *via* thiolation of bismuth, thus optimizing the pharmacokinetics profiles of oral bismuth drugs. In addition, NAC potentially widened the spectrum of inhibitory activities of bismuth drugs by increasing their accessibility to the biological targets that showed confined binding affinity to Bi^{3+}, *e.g.* ACE2. Notably, NAC was found to partially relieve lung pathology (Fig. 1G and H), which was probably due to its capacity to loosen thick mucus with chronic bronchopulmonary disorders.[56,58] Thus, NAC may also serve to broaden the therapeutic time window of CBS + 3NAC in either viral phase or inflammatory phase due to its antioxidant activity.[56]

Currently oral bismuth-containing drugs, *i.e.* BSS (Pepto-Bismol®) and CBS (De-Nol®, Lizhudele®) are in phase IV and III clinical trial (Clinical Trials Identifier: NCT04811339 and ChiCTR2000030398) respectively. The antiviral efficacies of
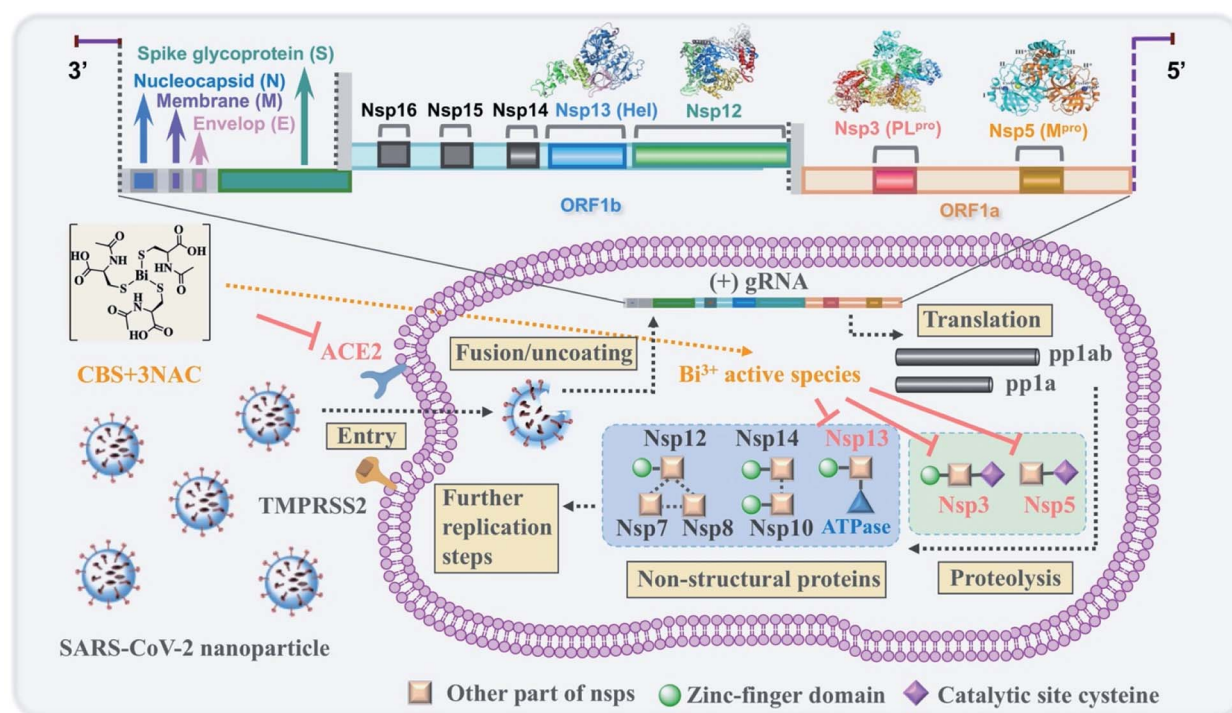
Scheme 1 Proposed molecular mechanism of action of CBS + 3NAC against SARS-CoV-2.

orally administered bismuth drugs are likely to be poor owing to their low systemic adsorption. By using the current strategy, the oral absorption of Bi^{3+} could be greatly improved, and the anti-ulcer bismuth drugs could be facilely and efficiently translated into orally available anti-CoVs agents. This study also augmented the therapeutic options of metal complexes as anti-CoVs agents. In a general way, soft or borderline metals are suitable to bind to the cysteine site of crucial viral proteins and interfere with the downstream biological events of viral replication steps. At low pH environment, chelation of metals by biologically compatible thiols or appropriate chelating ligands may represent one of the promising ways to enhance the solubility and permeability of the given cationic metal. We anticipate that more metal-based anti-CoV drug candidates could be discovered from screens after activity tests and toxicological assessments.

We have demonstrated that a cocktail therapy consisting of two clinically used drugs *i.e.*, CBS (or BSS) and NAC can serve as a promising orally administrated broad-spectrum anti-CoV regimen through targeting multiply crucial viral enzymes, providing a potential at-home treatment for combating SARS-CoV-2 and future coronavirus infections.

Ethical statement

All experiments were approved by, and performed in accordance with the guidelines approved by Committee on the Use of Live Animals in Teaching and Research (CULATR) of the University of Hong Kong.

Data availability

All experimental data and procedures are provided in the ESI.† Other data are available from the corresponding author upon reasonable request.

Author contributions

R. W., J. F.-W. C., H. L., J. Z., S. Y. and H. S. designed the experiments. T. K.-Y. I., S. W. and R. W. provided chemical stability data. S. W. and R. W. perform the *in vitro* and *ex vivo* permeability assay and analyzed the data. S. W., J. Z., and R. W. perform the *in vivo* mice and rat study and analyzed the data. S. Y. and J. F.-W. C. provided the *in vitro* and *in vivo* antiviral data. R. W. and S. W. provided all the data of enzyme-based study. R. W. and H. L. wrote the manuscript with inputs from H. S, J. F.-W. C. and S. Y. K.-Y. Y. and J. Z. Z provided conceptual advice and troubleshooting. H. S. and S. Y. supervised the study. H. S., S. Y. and J. F.-W. C. provided the grant support.

Conflicts of interest

H. S., K.-Y. Y., S. Y., R. W., H. L., J. F.-W. C., T. C. and S. W. have a pending patent application related to this manuscript. J. F.-W. C. has received travel grants from Pfizer Corporation Hong Kong and Astellas Pharma Hong Kong Corporation Limited and was an invited speaker for Gilead Sciences Hong Kong Limited

and Luminex Corporation. The other authors declare no competing interests.

Notes and references

1 World Health Organization, *Coronavirus Disease (COVID-19) Situation Reports*, https://www.who.int/emergencies/diseases/novel-coronavirus-2019/situation-reports, 2020.

2 B. S. Graham, *Science*, 2020, **368**, 945–946.

3 *Emerging SARS-CoV-2 variants*, Centers for Disease Control and Prevention, https://www.cdc.gov/coronavirus/2019-ncov/more/science-and-research/scientific-brief-emerging-variants.html#_ftn1, 2021.

4 A. Zumla, J. F. W. Chan, E. I. Azhar, D. S. C. Hui and K.-Y. Yuen, *Nat. Rev. Drug Discovery*, 2016, **15**, 327–347.

5 J. H. Beigel, K. M. Tomashek and L. E. Dodd, *N. Engl. J. Med.*, 2020, **383**, 994.

6 J. D. Goldman, D. C. B. Lye, D. S. Hui, K. M. Marks, R. Bruno, R. Montejano, C. D. Spinner, M. Galli, K. T. Tashima, G. Diaz, A. Subramanian, *et al.*, *N. Engl. J. Med.*, 2020, **383**, 1827–1837.

7 I. F. Hung, K. C. Lung, E. Y. Tso, R. Liu, T. W. Chung, M. Y. Chu, Y. Y. Ng, J. Lo, J. Chan, A. R. Tam, T. L. Que, C. S. Lau, K. H. Chan, K. K. To, K. Y. Yuen, *et al.*, *Lancet*, 2020, **395**, 1695–1704.

8 K. Kupferschmidt and J. Cohen, *Science*, 2020, **367**, 1412–1413.

9 S. F. Yuan, R. M. Wang, J. F. W. Chan, A. J. X. Zhang, T. F. Cheng, K. K. H. Chik, Z. W. Ye, S. Y. Wang, L. J. Jin, H. Y. Li, D. Y. Jin, K. Y. Yuen and H. Z. Sun, *Nat. Microbiol.*, 2020, **5**, 1439–1448.

10 J. F.-W. Chan, A. J. Zhang, S. Yuan, V. K.-M. Poon, C. C.-S. Chan, A. C.-Y. Lee, W.-M. Chan, Z. Fan, K. K.-W. To, K.-Y. Yuen, *et al.*, *Clin. Infect. Dis.*, 2020, **71**, 2428–2446.

11 E. Mahase, *Br. Med. J.*, 2019, **367**, l5832.

12 H. Li, R. Wang and H. Sun, *Acc. Chem. Res.*, 2019, **52**, 216–227.

13 Y. Hong, Y.-T. Lai, G. C.-F. Chan and H. Sun, *Proc. Natl. Acad. Sci. U. S. A.*, 2015, **112**, 3211.

14 P. J. Sadler, H. Sun and H. Li, *Chem.–Eur. J.*, 1996, **2**, 701–708.

15 L. F. Prescott, R. N. Illingworth, J. A. Critchley, M. J. Stewart, R. D. Adam and A. T. Proudfoot, *Br. Med. J.*, 1979, **2**, 1097–1100.

16 J. Geiler, M. Michaelis, P. Naczk, A. Leutz, K. Langer, H.-W. Doerr and J. Cinatl, *Biochem. Pharmacol.*, 2010, **79**, 413–420.

17 B. Meng, S. A. Kemp, G. Papa, R. Datir, I. Ferreira, S. Marelli, W. T. Harvey, S. Lytras, A. Mohamed, G. Gallo, N. Thakur, D. A. Collier and P. Mlcochova, *Cell Rep.*, 2021, **35**(13), 109292.

18 H. Sun, H. Li, I. Harvey and P. J. Sadler, *J. Biol. Chem.*, 1999, **274**, 29094–29101.

19 J. Ye, A. J. Chu, R. Harper, S. T. Chan, T. L. Shek, Y. Zhang, M. Ip, M. Sambir, I. Artsimovitch, Z. Zuo, X. Yang and C. Ma, *J. Med. Chem.*, 2020, **63**, 7695–7720.

20 M. A. Alam, F. I. Al-Jenoobi and A. M. Al-mohizea, *J. Pharm. Pharmacol.*, 2011, **64**, 326–336.

21 B. T. Leussink, A. Slikkerveer, W. J. J. Krauwinkel, G. B. van der Voet, E. de Heer, F. A. de Wolff and J. A. Bruijn, *Arch. Toxicol.*, 2000, **74**, 349–355.

22 W. Hespe, H. J. M. Staal and D. W. R. Hall, *Lancet*, 1988, **332**, 1258.

23 J. Lei, Y. Kusov and R. Hilgenfeld, *Antiviral Res.*, 2018, **149**, 58–74.

24 H. Li and H. Sun, *Curr. Opin. Chem. Biol.*, 2012, **16**, 74–83.

25 P. Malfertheiner, F. Bazzoli, J. C. Delchier, K. Celinski, M. Giguere, M. Riviere and F. Megraud, *Lancet*, 2011, **377**, 905–913.

26 D. M. Griffith, H. Y. Li, M. V. Werrett, P. C. Andrews and H. Sun, *Chem. Soc. Rev.*, 2021, **50**, 12037–12069.

27 R. Mohan, *Nat. Chem.*, 2010, **2**, 336.

28 L. A. Tillman, F. M. Drake, J. S. Dixon and J. R. Wood, *Aliment. Pharmacol. Ther.*, 1996, **10**, 459–467.

29 A. C. Ford, P. Malfertheiner, M. Giguere, J. Santana, M. Khan and P. Moayyedi, *World J. Gastroenterol.*, 2008, **14**, 7361–7370.

30 E. G. Taylor and P. Klenerman, *Lancet*, 1990, **335**, 670–671.

31 M. Sarikaya, A. Sevinc, R. Ulu, F. Ates and F. Ari, *Nephron*, 2002, **90**, 501–502.

32 K. D. McCormick, J. L. Jacobs and J. W. Mellors, *Science*, 2021, **371**, 1306.

33 M. K. Lo, C. G. Albariño, J. K. Perry, S. Chang, E. P. Tchesnokov, L. Guerrero, A. Chakrabarti, P. Shrivastava-Ranjan, C. F. Spiropoulou, *et al.*, *Proc. Natl. Acad. Sci. U. S. A.*, 2020, **117**, 26946.

34 L. A. Tillman, F. M. Drake, J. S. Dixon and J. R. Wood, *Aliment. Pharmacol. Ther.*, 1996, **10**, 459–467.

35 J. R. Lambert and P. Midolo, *Aliment. Pharmacol. Ther.*, 1997, **11**(Suppl 1), 27–33.

36 A. Slikkerveer, R. B. Helmich, G. B. van Der Voet and F. A. de Wolff, *J. Pharm. Sci.*, 1995, **84**, 512–515.

37 D. R. Williams, *J. Inorg. Nucl. Chem.*, 1977, **39**, 711–714.

38 P. J. Sadler and H. Sun, *J. Chem. Soc., Dalton Trans.*, 1995, 1395–1401.

39 W. Li, L. Jin, N. Zhu, X. Hou, F. Deng and H. Sun, *J. Am. Chem. Soc.*, 2003, **125**, 12408–12409.

40 C. F. Baes and R. S. Mesmer, *Ber. Bunsenges. Phys. Chem.*, 1977, **81**, 245–246.

41 G. G. Briand, N. Burford, M. D. Eelman, N. Aumeerally, L. Chen, T. S. Cameron and K. N. Robertson, *Inorg. Chem.*, 2004, **43**, 6495–6500.

42 H. Sun, H. Li, I. Harvey and P. J. Sadler, *J. Biol. Chem.*, 1999, **274**, 29094–29101.

43 A. J. Wagstaff, P. Benfield and J. P. Monk, *Drugs*, 1988, **36**, 132–157.

44 R. Wang, H. Li, T. K.-Y. Ip and H. Sun, in *Adv. Inorg. Chem.*, ed. P. J. Sadler and R. van Eldik, Academic Press, 2020, vol. 75, pp. 183–205.

45 P. Domenico, R. J. Salo, S. G. Novick, P. E. Schoch, K. Van Horn and B. A. Cunha, *Antimicrob. Agents Chemother.*, 1997, **41**, 1697–1703.

46 A. Karbasi, S. Hossein Hosseini, M. Shohrati, M. Amini and B. Najafian, *Minerva Dietol. Gastroenterol.*, 2013, **59**, 107–112.

47 N. Yang, J. A. Tanner, B.-J. Zheng, R. M. Watt, M.-L. He, L.-Y. Lu, J.-Q. Jiang, K.-T. Shum, Y.-P. Lin, K.-L. Wong, M. C. M. Lin, H.-F. Kung, H. Sun and J.-D. Huang, *Angew. Chem., Int. Ed.*, 2007, **46**, 6464–6468.

48 R. Wang, T.-P. Lai, P. Gao, H. Zhang, P.-L. Ho, P. C.-Y. Woo, G. Ma, R. Y.-T. Kao, H. Li and H. Sun, *Nat. Commun.*, 2018, **9**, 439.

49 S. Cun and H. Sun, *Proc. Natl. Acad. Sci. U. S. A.*, 2010, **107**, 4943.

50 S. Cun, H. Li, R. Ge, M. C. M. Lin and H. Sun, *J. Biol. Chem.*, 2008, **283**, 15142–15151.

51 R. Wang, S. Wang, S. Chan, Y. Wang, Y. Zhang, Z. Zuo, G. Chi-Fung Chan, H. Li and H. Sun, *iScience*, 2020, **23**, 101054.

52 A. Zoufaly, M. Poglitsch, J. H. Aberle, W. Hoepler, T. Seitz, M. Traugott, A. Grieb, E. Pawelka, A. S. Slutsky, J. M. Penninger, *et al.*, *Lancet Respir. Med.*, 2020, **8**, 1154–1158.

53 H. Sun, Q. Zhang, R. Wang, H. Wang, Y.-T. Wong, M. Wang, Q. Hao, A. Yan, R. Y.-T. Kao, P.-L. Ho and H. Li, *Nat. Commun.*, 2020, **11**, 5263.

54 L. F. Prescott, J. Park, A. Ballantyne, P. Adriaenssens and A. T. Proudfoot, *Lancet*, 1977, **2**, 432–434.

55 M. J. Smilkstein, G. L. Knapp, K. W. Kulig and B. H. Rumack, *N. Engl. J. Med.*, 1988, **319**, 1557–1562.

56 F. O. Omara, B. R. Blakley, J. Bernier and M. Fournier, *Toxicology*, 1997, **116**, 219–226.

57 Z. Shi and C. A. Puyo, *Ther. Clin. Risk Manage.*, 2020, **16**, 1047–1055.

58 P. N. R. Dekhuijzen, *Eur. Respir. J.*, 2004, **23**, 629–636.